Search for first-generation leptoquarks at HERA

H. Abramowicz *et al.* (ZEUS Collaboration)

Phys. Rev. D **86**, 012005 — Published 18 July 2012

DOI: 10.1103/PhysRevD.86.012005

DESY–12–077

Search for first-generation leptoquarks at HERA

ZEUS Collaboration

Abstract

A search for first-generation leptoquarks was performed in electron-proton and positron-proton collisions recorded with the ZEUS detector at HERA in 2003–2007 using an integrated luminosity of 366 pb^{-1}. Final states with an electron and jets or with missing transverse momentum and jets were analysed, searching for resonances or other deviations from the Standard Model predictions. No evidence for any leptoquark signal was found. The data were combined with data previously taken at HERA, resulting in a total integrated luminosity of 498 pb^{-1}. Limits on the Yukawa coupling, λ, of leptoquarks were set as a function of the leptoquark mass for different leptoquark types within the Buchmüller-Rückl-Wyler model. Leptoquarks with a coupling $\lambda = 0.3$ are excluded for masses up to 699 GeV.

The ZEUS Collaboration

H. Abramowicz[45,aj], I. Abt[35], L. Adamczyk[13], M. Adamus[54], R. Aggarwal[7,c], S. Antonelli[4], P. Antonioli[3], A. Antonov[33], M. Arneodo[50], O. Arslan[5], V. Aushev[26,27,aa], Y. Aushev,[27,aa,ab], O. Bachynska[15], A. Bamberger[19], A.N. Barakbaev[25], G. Barbagli[17], G. Bari[3], F. Barreiro[30], N. Bartosik[15], D. Bartsch[5], M. Basile[4], O. Behnke[15], J. Behr[15], U. Behrens[15], L. Bellagamba[3], A. Bertolin[39], S. Bhadra[57], M. Bindi[4], C. Blohm[15], V. Bokhonov[26,aa], T. Bołd[13], K. Bondarenko[27], E.G. Boos[25], K. Borras[15], D. Boscherini[3], D. Bot[15], I. Brock[5], E. Brownson[56], R. Brugnera[40], N. Brümmer[37], A. Bruni[3], G. Bruni[3], B. Brzozowska[53], P.J. Bussey[20], B. Bylsma[37], A. Caldwell[35], M. Capua[8], R. Carlin[40], C.D. Catterall[57], S. Chekanov[1], J. Chwastowski[12,e], J. Ciborowski[53,an], R. Ciesielski[15,h], L. Cifarelli[4], F. Cindolo[3], A. Contin[4], A.M. Cooper-Sarkar[38], N. Coppola[15,i], M. Corradi[3], F. Corriveau[31], M. Costa[49], G. D'Agostini[43], F. Dal Corso[39], J. del Peso[30], R.K. Dementiev[34], S. De Pasquale[4,a], M. Derrick[1], R.C.E. Devenish[38], D. Dobur[19,t], B.A. Dolgoshein [33,†], G. Dolinska[27], A.T. Doyle[20], V. Drugakov[16], L.S. Durkin[37], S. Dusini[39], Y. Eisenberg[55], P.F. Ermolov [34,†], A. Eskreys [12,†], S. Fang[15,j], S. Fazio[8], J. Ferrando[38], M.I. Ferrero[49], J. Figiel[12], M. Forrest[20,w], B. Foster[38,ae], G. Gach[13], A. Galas[12], E. Gallo[17], A. Garfagnini[40], A. Geiser[15], I. Gialas[21,x], A. Gizhko[27,ac], L.K. Gladilin[34,ad], D. Gladkov[33], C. Glasman[30], O. Gogota[27], Yu.A. Golubkov[34], P. Göttlicher[15,k], I. Grabowska-Bołd[13], J. Grebenyuk[15], I. Gregor[15], G. Grigorescu[36], G. Grzelak[53], O. Gueta[45], M. Guzik[13], C. Gwenlan[38,af], T. Haas[15], W. Hain[15], R. Hamatsu[48], J.C. Hart[44], H. Hartmann[5], G. Hartner[57], E. Hilger[5], D. Hochman[55], R. Hori[47], K. Horton[38,ag], A. Hüttmann[15], Z.A. Ibrahim[10], Y. Iga[42], R. Ingbir[45], M. Ishitsuka[46], H.-P. Jakob[5], F. Januschek[15], T.W. Jones[52], M. Jüngst[5], I. Kadenko[27], B. Kahle[15], S. Kananov[45], T. Kanno[46], U. Karshon[55], F. Karstens[19,u], I.I. Katkov[15,l], M. Kaur[7], P. Kaur[7,c], A. Keramidas[36], L.A. Khein[34], J.Y. Kim[9], D. Kisielewska[13], S. Kitamura[48,al], R. Klanner[22], U. Klein[15,m], E. Koffeman[36], N. Kondrashova[27,ac], O. Kononenko[27], P. Kooijman[36], Ie. Korol[27], I.A. Korzhavina[34,ad], A. Kotański[14,f], U. Kötz[15], H. Kowalski[15], O. Kuprash[15], M. Kuze[46], A. Lee[37], B.B. Levchenko[34], A. Levy[45], V. Libov[15], S. Limentani[40], T.Y. Ling[37], M. Lisovyi[15], E. Lobodzinska[15], W. Lohmann[16], B. Löhr[15], E. Lohrmann[22], K.R. Long[23], A. Longhin[39,ah], D. Lontkovskyi[15], O.Yu. Lukina[34], J. Maeda[46,ak], S. Magill[1], I. Makarenko[15], J. Malka[15], R. Mankel[15], A. Margotti[3], G. Marini[43], J.F. Martin[51], A. Mastroberardino[8], M.C.K. Mattingly[2], I.-A. Melzer-Pellmann[15], S. Mergelmeyer[5], S. Miglioranzi[15,n], F. Mohamad Idris[10], V. Monaco[49], A. Montanari[15], J.D. Morris[6,b], K. Mujkic[15,o], B. Musgrave[1], K. Nagano[24], T. Namsoo[15,p], R. Nania[3], A. Nigro[43], Y. Ning[11], T. Nobe[46], D. Notz[15], R.J. Nowak[53], A.E. Nuncio-Quiroz[5], B.Y. Oh[41], N. Okazaki[47], K. Oliver[38], K. Olkiewicz[12], Yu. Onishchuk[27], K. Papageorgiu[21], A. Parenti[15], E. Paul[5], J.M. Pawlak[53], B. Pawlik[12], P. G. Pelfer[18], A. Pellegrino[36], W. Perlański[53,ao], H. Perrey[15], K. Piotrzkowski[29], P. Pluciński[54,ap], N.S. Pokrovskiy[25], A. Polini[3], A.S. Proskuryakov[34], M. Przybycień[13], A. Raval[15], D.D. Reeder[56], B. Reisert[35], Z. Ren[11], J. Repond[1], Y.D. Ri[48,am], A. Robertson[38], P. Roloff[15,n], I. Rubinsky[15], M. Ruspa[50], R. Sacchi[49], U. Samson[5], G. Sartorelli[4], A.A. Savin[56], D.H. Saxon[20], M. Schioppa[8], S. Schlenstedt[16], P. Schleper[22], W.B. Schmidke[35], U. Schneekloth[15], V. Schönberg[5], T. Schörner-Sadenius[15], J. Schwartz[31], F. Sciulli[11], L.M. Shcheglova[34], R. Shehzadi[5], S. Shimizu[47,n], I. Singh[7,c], I.O. Skillicorn[20], W. Słomiński[14,g], W.H. Smith[56], V. Sola[22], A. Solano[49], D. Son[28], V. Sosnovtsev[33], A. Spiridonov[15,q], H. Stadie[22], L. Stanco[39], N. Stefaniuk[27], A. Stern[45], T.P. Stewart[51], A. Stifutkin[33], P. Stopa[12], S. Suchkov[33], G. Susinno[8], L. Suszycki[13], J. Sztuk-Dambietz[22], D. Szuba[22], J. Szuba[15,r], A.D. Tapper[23], E. Tassi[8,d], J. Terrón[30], T. Theedt[15], H. Tiecke[36], K. Tokushuku[24,y], J. Tomaszewska[15,s], V. Trusov[27], T. Tsurugai[32], M. Turcato[22], O. Turkot[27,ac], T. Tymieniecka[54,aq], M. Vázquez[36,n], A. Verbytskyi[15], O. Viazlo[27], N.N. Vlasov[19,v], R. Walczak[38], W.A.T. Wan Abdullah[10], J.J. Whitmore[41,ai],

K. Wichmann[15], L. Wiggers[36], M. Wing[52], M. Wlasenko[5], G. Wolf[15], H. Wolfe[56], K. Wrona[15], A.G. Yagües-Molina[15], S. Yamada[24], Y. Yamazaki[24,z], R. Yoshida[1], C. Youngman[15], O. Zabiegalov[27,ac], A.F. Żarnecki[53], L. Zawiejski[12], O. Zenaiev[15], W. Zeuner[15,n], B.O. Zhautykov[25], N. Zhmak[26,aa], C. Zhou[31], A. Zichichi[4], Z. Zolkapli[10], D.S. Zotkin[34]

[1] *Argonne National Laboratory, Argonne, Illinois 60439-4815, USA* [A]
[2] *Andrews University, Berrien Springs, Michigan 49104-0380, USA*
[3] *INFN Bologna, Bologna, Italy* [B]
[4] *University and INFN Bologna, Bologna, Italy* [B]
[5] *Physikalisches Institut der Universität Bonn, Bonn, Germany* [C]
[6] *H.H. Wills Physics Laboratory, University of Bristol, Bristol, United Kingdom* [D]
[7] *Panjab University, Department of Physics, Chandigarh, India*
[8] *Calabria University, Physics Department and INFN, Cosenza, Italy* [B]
[9] *Institute for Universe and Elementary Particles, Chonnam National University, Kwangju, South Korea*
[10] *Jabatan Fizik, Universiti Malaya, 50603 Kuala Lumpur, Malaysia* [E]
[11] *Nevis Laboratories, Columbia University, Irvington on Hudson, New York 10027, USA* [F]
[12] *The Henryk Niewodniczanski Institute of Nuclear Physics, Polish Academy of Sciences, Krakow, Poland* [G]
[13] *AGH-University of Science and Technology, Faculty of Physics and Applied Computer Science, Krakow, Poland* [H]
[14] *Department of Physics, Jagellonian University, Cracow, Poland*
[15] *Deutsches Elektronen-Synchrotron DESY, Hamburg, Germany*
[16] *Deutsches Elektronen-Synchrotron DESY, Zeuthen, Germany*
[17] *INFN Florence, Florence, Italy* [B]
[18] *University and INFN Florence, Florence, Italy* [B]
[19] *Fakultät für Physik der Universität Freiburg i.Br., Freiburg i.Br., Germany*
[20] *School of Physics and Astronomy, University of Glasgow, Glasgow, United Kingdom* [D]
[21] *Department of Engineering in Management and Finance, Univ. of the Aegean, Chios, Greece*
[22] *Hamburg University, Institute of Experimental Physics, Hamburg, Germany* [I]
[23] *Imperial College London, High Energy Nuclear Physics Group, London, United Kingdom* [D]
[24] *Institute of Particle and Nuclear Studies, KEK, Tsukuba, Japan* [J]
[25] *Institute of Physics and Technology of Ministry of Education and Science of Kazakhstan, Almaty, Kazakhstan*
[26] *Institute for Nuclear Research, National Academy of Sciences, Kyiv, Ukraine*
[27] *Department of Nuclear Physics, National Taras Shevchenko University of Kyiv, Kyiv, Ukraine*
[28] *Kyungpook National University, Center for High Energy Physics, Daegu, South Korea* [K]
[29] *Institut de Physique Nucléaire, Université Catholique de Louvain, Louvain-la-Neuve, Belgium* [L]
[30] *Departamento de Física Teórica, Universidad Autónoma de Madrid, Madrid, Spain* [M]
[31] *Department of Physics, McGill University, Montréal, Québec, Canada H3A 2T8* [N]
[32] *Meiji Gakuin University, Faculty of General Education, Yokohama, Japan* [J]
[33] *Moscow Engineering Physics Institute, Moscow, Russia* [O]
[34] *Lomonosov Moscow State University, Skobeltsyn Institute of Nuclear Physics, Moscow, Russia* [P]
[35] *Max-Planck-Institut für Physik, München, Germany*

[36] *NIKHEF and University of Amsterdam, Amsterdam, Netherlands* [Q]
[37] *Physics Department, Ohio State University, Columbus, Ohio 43210, USA* [A]
[38] *Department of Physics, University of Oxford, Oxford, United Kingdom* [D]
[39] *INFN Padova, Padova, Italy* [B]
[40] *Dipartimento di Fisica dell' Università and INFN, Padova, Italy* [B]
[41] *Department of Physics, Pennsylvania State University, University Park, Pennsylvania 16802, USA* [F]
[42] *Polytechnic University, Tokyo, Japan* [J]
[43] *Dipartimento di Fisica, Università 'La Sapienza' and INFN, Rome, Italy* [B]
[44] *Rutherford Appleton Laboratory, Chilton, Didcot, Oxon, United Kingdom* [D]
[45] *Raymond and Beverly Sackler Faculty of Exact Sciences, School of Physics, Tel Aviv University, Tel Aviv, Israel* [R]
[46] *Department of Physics, Tokyo Institute of Technology, Tokyo, Japan* [J]
[47] *Department of Physics, University of Tokyo, Tokyo, Japan* [J]
[48] *Tokyo Metropolitan University, Department of Physics, Tokyo, Japan* [J]
[49] *Università di Torino and INFN, Torino, Italy* [B]
[50] *Università del Piemonte Orientale, Novara, and INFN, Torino, Italy* [B]
[51] *Department of Physics, University of Toronto, Toronto, Ontario, Canada M5S 1A7* [N]
[52] *Physics and Astronomy Department, University College London, London, United Kingdom* [D]
[53] *Faculty of Physics, University of Warsaw, Warsaw, Poland*
[54] *National Centre for Nuclear Research, Warsaw, Poland*
[55] *Department of Particle Physics and Astrophysics, Weizmann Institute, Rehovot, Israel*
[56] *Department of Physics, University of Wisconsin, Madison, Wisconsin 53706, USA* [A]
[57] *Department of Physics, York University, Ontario, Canada M3J 1P3* [N]

[A] supported by the US Department of Energy
[B] supported by the Italian National Institute for Nuclear Physics (INFN)
[C] supported by the German Federal Ministry for Education and Research (BMBF), under contract No. 05 H09PDF
[D] supported by the Science and Technology Facilities Council, UK
[E] supported by an FRGS grant from the Malaysian government
[F] supported by the US National Science Foundation. Any opinion, findings and conclusions or recommendations expressed in this material are those of the authors and do not necessarily reflect the views of the National Science Foundation.
[G] supported by the Polish Ministry of Science and Higher Education as a scientific project No. DPN/N188/DESY/2009
[H] supported by the Polish Ministry of Science and Higher Education and its grants for Scientific Research
[I] supported by the German Federal Ministry for Education and Research (BMBF), under contract No. 05h09GUF, and the SFB 676 of the Deutsche Forschungsgemeinschaft (DFG)
[J] supported by the Japanese Ministry of Education, Culture, Sports, Science and Technology (MEXT) and its grants for Scientific Research
[K] supported by the Korean Ministry of Education and Korea Science and Engineering Foundation
[L] supported by FNRS and its associated funds (IISN and FRIA) and by an Inter-University Attraction Poles Programme subsidised by the Belgian Federal Science Policy Office
[M] supported by the Spanish Ministry of Education and Science through funds provided by CICYT
[N] supported by the Natural Sciences and Engineering Research Council of Canada (NSERC)
[O] partially supported by the German Federal Ministry for Education and Research (BMBF)
[P] supported by RF Presidential grant N 4142.2010.2 for Leading Scientific Schools, by the Russian Ministry of Education and Science through its grant for Scientific Research on High Energy Physics and under contract No.02.740.11.0244
[Q] supported by the Netherlands Foundation for Research on Matter (FOM)
[R] supported by the Israel Science Foundation

[a] now at University of Salerno, Italy
[b] now at Queen Mary University of London, United Kingdom
[c] also funded by Max Planck Institute for Physics, Munich, Germany
[d] also Senior Alexander von Humboldt Research Fellow at Hamburg University, Institute of Experimental Physics, Hamburg, Germany
[e] also at Cracow University of Technology, Faculty of Physics, Mathemathics and Applied Computer Science, Poland
[f] supported by the research grant No. 1 P03B 04529 (2005-2008)
[g] supported by the Polish National Science Centre, project No. DEC-2011/01/BST2/03643
[h] now at Rockefeller University, New York, NY 10065, USA
[i] now at DESY group FS-CFEL-1
[j] now at Institute of High Energy Physics, Beijing, China
[k] now at DESY group FEB, Hamburg, Germany
[l] also at Moscow State University, Russia
[m] now at University of Liverpool, United Kingdom
[n] now at CERN, Geneva, Switzerland
[o] also affiliated with Universtiy College London, UK
[p] now at Goldman Sachs, London, UK
[q] also at Institute of Theoretical and Experimental Physics, Moscow, Russia
[r] also at FPACS, AGH-UST, Cracow, Poland
[s] partially supported by Warsaw University, Poland
[t] now at Istituto Nucleare di Fisica Nazionale (INFN), Pisa, Italy
[u] now at Haase Energie Technik AG, Neumünster, Germany
[v] now at Department of Physics, University of Bonn, Germany
[w] now at Biodiversität und Klimaforschungszentrum (BiK-F), Frankfurt, Germany
[x] also affiliated with DESY, Germany
[y] also at University of Tokyo, Japan
[z] now at Kobe University, Japan
[†] deceased
[aa] supported by DESY, Germany
[ab] member of National Technical University of Ukraine, Kyiv Polytechnic Institute, Kyiv, Ukraine
[ac] member of National University of Kyiv - Mohyla Academy, Kyiv, Ukraine
[ad] partly supported by the Russian Foundation for Basic Research, grant 11-02-91345-DFG_a
[ae] Alexander von Humboldt Professor; also at DESY and University of Oxford
[af] STFC Advanced Fellow
[ag] nee Korcsak-Gorzo
[ah] now at LNF, Frascati, Italy
[ai] This material was based on work supported by the National Science Foundation, while working at the Foundation.
[aj] also at Max Planck Institute for Physics, Munich, Germany, External Scientific Member
[ak] now at Tokyo Metropolitan University, Japan
[al] now at Nihon Institute of Medical Science, Japan
[am] now at Osaka University, Osaka, Japan

[an] also at Łódź University, Poland
[ao] member of Łódź University, Poland
[ap] now at Department of Physics, Stockholm University, Stockholm, Sweden
[aq] also at Cardinal Stefan Wyszyński University, Warsaw, Poland

1 Introduction

Many extensions of the Standard Model (SM) predict the existence of particles carrying both baryon and lepton number, such as leptoquarks (LQs) [1]. In ep collisions at HERA, such states could have been produced directly through electron[1]-quark fusion (Fig. 1a) if their masses, $M_{\rm LQ}$, were lower than the HERA centre-of-mass energy, $\sqrt{s}$. The leptoquarks would have decayed into an electron and quark or an electron neutrino and quark, yielding peaks in the spectra of the final-state lepton-jets[2] invariant mass, M_{ljs}. Leptoquarks with $M_{\rm LQ} > \sqrt{s}$ could not have been produced as resonances, but they would still have caused deviations from the SM prediction in the observed M_{ljs} spectrum due to virtual LQ exchange (Fig. 1a and b). This paper presents an analysis of the M_{ljs} spectrum searching for evidence for leptoquarks.

The prediction for the M_{ljs} spectrum is given by SM neutral current (NC) and charged current (CC) deep inelastic scattering (DIS) (Fig. 1c). Any leptoquark signal would have to be identified as a deviation from this SM prediction. At high M_{ljs}, the SM prediction falls rapidly due to the dependence of the DIS cross sections on Q^2, the virtuality of the exchanged boson, and to the sharply falling valence-quark density at large Bjorken x. This makes the data especially sensitive to virtual leptoquark exchange and LQ-DIS interference.

Leptoquarks have been searched for previously in ep collisions [2–5] and in e^+e^- [6, 7], $p\bar{p}$ [8, 9] and pp [10–12] collisions. Using ep collisions, the Yukawa coupling, λ, of possible LQ states to electron and electron neutrino is probed. In $p\bar{p}$ and pp collisions, the LQ production proceeds via the strong interaction and is independent of λ. Thus the experimental approaches are complementary and ep collisions provide a unique testing ground. For this paper, the predictions for LQ cross sections were determined in leading order (LO) using the CTEQ5D parton density functions [13] (PDFs) using the Buchmüller-Rückl-Wyler model [1]. This model assumes that some of the leptoquarks are doublets or triplets with degenerate masses. This differs from the assumptions made for production via the strong interaction where in general a singlet state is assumed. The LHC experiments so far provided only limits for scalar LQs [10–12].

In the analysis presented here, no evidence for any leptoquark signal was found. Therefore limits on λ were derived as a function of $M_{\rm LQ}$ for the different leptoquark states described by the Buchmüller-Rückl-Wyler model.

The analysis is based on the data collected by the ZEUS experiment in the period 2003–2007, corresponding to an integrated luminosity of 366 pb^{-1}. During this period, HERA was operated with a polarised lepton beam. The four data subsamples with different polarisation and lepton beam charge are summarised in Table 1. The experimental set-up described in Section 2 is that corresponding to these subsamples. The final limits set also

[1] Unless otherwise specified, 'electron' refers to both positron and electron and 'neutrino' refers to both neutrino and antineutrino.

[2] There can be more than one jet in the final state due to QCD initial or final state radiation.

included data collected in 1994–2000, giving a total integrated luminosity of 498 pb^{-1}. Thus all data from ZEUS were included and the results presented here supersede those published previously [2–4].

2 Experimental set-up

A detailed description of the ZEUS detector can be found elsewhere [14]. A brief outline of the components that are most relevant for this analysis is given below.

In the kinematic range of the analysis, charged particles were tracked in the central tracking detector (CTD) [15] and the microvertex detector (MVD) [16]. These components operated in a magnetic field of 1.43 T provided by a thin superconducting solenoid. The CTD consisted of 72 cylindrical drift-chamber layers, organised in nine superlayers covering the polar-angle [3] region $15^\circ < \theta < 164^\circ$. The MVD silicon tracker consisted of a barrel (BMVD) and a forward (FMVD) section. The BMVD contained three layers and provided polar-angle coverage for tracks from 30° to 150°. The four-layer FMVD extended the polar-angle coverage in the forward region to 7°. After alignment, the single-hit resolution of the MVD was 24 μm. The transverse distance of closest approach (DCA) to the nominal vertex in X–Y was measured to have a resolution, averaged over the azimuthal angle, of $(46 \oplus 122/p_T)$ μm, with p_T in GeV. For CTD-MVD tracks that pass through all nine CTD superlayers, the momentum resolution was $\sigma(p_T)/p_T = 0.0029p_T \oplus 0.0081 \oplus 0.0012/p_T$, with p_T in GeV.

The high-resolution uranium–scintillator calorimeter (CAL) [17] consisted of three parts: the forward (FCAL), the barrel (BCAL) and the rear (RCAL) calorimeters. Each part was subdivided transversely into towers and longitudinally into one electromagnetic section (EMC) and either one (in RCAL) or two (in BCAL and FCAL) hadronic sections (HAC). The smallest subdivision of the calorimeter was called a cell. The CAL energy resolutions, as measured under test-beam conditions, were $\sigma(E)/E = 0.18/\sqrt{E}$ for electrons and $\sigma(E)/E = 0.35/\sqrt{E}$ for hadrons, with E in GeV.

The luminosity was measured using the Bethe-Heitler reaction $ep \to e\gamma p$ by a luminosity detector which consisted of independent lead–scintillator calorimeter [18] and magnetic spectrometer [19] systems.

The lepton beam in HERA became naturally transversely polarised through the Sokolov-Ternov effect [20, 21]. The characteristic build-up time for the HERA accelerator was approximately 40 minutes. Spin rotators on either side of the ZEUS detector changed the transverse polarisation of the beam into longitudinal polarisation and back again. The lepton beam polarisation was measured using two independent polarimeters, the

[3] The ZEUS coordinate system is a right-handed Cartesian system, with the Z axis pointing in the nominal proton beam direction, referred to as the "forward direction", and the X axis pointing towards the centre of HERA. The coordinate origin is at the centre of the CTD. The pseudorapidity is defined as $\eta = -\ln\left(\tan\frac{\theta}{2}\right)$, where the polar angle, θ, is measured with respect to the Z axis.

transverse polarimeter (TPOL) [22] and the longitudinal polarimeter (LPOL) [23]. Both devices exploited the spin-dependent cross section for Compton scattering of circularly polarised photons off electrons to measure the beam polarisation. The luminosity and polarisation measurements were made over time intervals that were much shorter than the polarisation build-up time. The polarisation values measured in different data taking periods are shown in Table 1. The fractional systematic uncertainty on the measured polarisation was 4.2% for TPOL and 3.6% for LPOL.

3 Monte Carlo simulation

Monte Carlo techniques were used to determine the SM DIS background and the M_{ljs} resolution of a possible signal.

Standard Model NC and CC DIS events were simulated using the HERACLES 4.6.6 [24] program with the DJANGOH 1.6 [25] interfaces to the hadronisation programs and using CTEQ5D [13] PDFs. Radiative corrections for initial- and final-state electroweak radiation, vertex and propagator corrections, and two-boson exchange were included. The colour-dipole model of ARIADNE 4.12 [26] was used to simulate $\mathcal{O}(\alpha_S)$ plus leading-logarithmic corrections to the result of the quark-parton model. ARIADNE uses the Lund string model of JETSET 7.4.1 [27] for the hadronisation.

The production and decay of resonances were simulated using PYTHIA 6.1 [28], which takes into account the finite width of the resonant state, but includes only the s-channel diagrams. It also takes into account initial- and final-state QCD radiation from the quark and the effect of LQ hadronisation before decay [29] as well as the initial-state QED radiation from the electron. Such simulated samples of LQ events were used to study the bias and the resolution for the reconstructed LQ mass. The prediction for a LQ contribution to the DIS samples was evaluated by reweighting the DIS samples according to the LQ production processes (Section 6).

The ZEUS detector response was simulated using a program based on GEANT 3.21 [30]. The generated events were passed through the detector simulation, subjected to the same trigger requirements as the data and processed by the same reconstruction programs.

4 Leptoquark signal expectation

The Buchmüller-Rückl-Wyler (BRW) model [1] was used to calculate the cross sections in LO using the CTEQ5D PDFs for the LQ states listed in Table 2. The next-to-leading-order (NLO) QCD corrections, the so-called K-factors [31, 32], available for scalar LQs were not considered, because equivalent calculations are not available for vector LQs. All limits presented in this paper are for LQ production in this model. As the K-factors

are typically of the order of 1.2, the final limits on λ would be more stringent by about 10% if the K-factors were applied.

As the final states for LQ production are identical to states produced in DIS, the DIS Monte Carlo samples were reweighted accordingly to produce predictions for the respective M_{ljs} spectra. The BRW model predicts a dependence of the cross sections on the beam polarisation. Therefore predictions were computed taking into account the average polarisation of the respective data samples.

The BRW model includes both u and s channel and interferences with DIS. For $M_{\mathrm{LQ}} > \sqrt{s}$, the full LQ cross sections were used. For the virtual exchange, the cross section has a λ^4 dependence. The interference terms provide a contribution with a λ^2 dependence. For $M_{\mathrm{LQ}} < \sqrt{s}$, some simplifications were introduced. While the interference terms were calculated as for large M_{LQ}, the u-channel contribution, expected to be small, was neglected and the narrow-width approximation (NWA) was used for the resonant s-channel LQ production. The effect of the simplifications on the final limits on λ is well below 10%.

The Born-level cross section for the resonant (s-channel) LQ production in the NWA is:

$$\sigma^{\mathrm{NWA}} = (J+1)\frac{\pi}{4s}\lambda^2\, q(x_0, M_{\mathrm{LQ}}^2)(1 \pm P_e),$$

where $q(x_0, M_{\mathrm{LQ}}^2)$ is the initial-state quark (or antiquark) parton-density function in the proton for $x_0 = M_{\mathrm{LQ}}^2/s$, J is the spin of the LQ and the term $1 \pm P_e$ accounts for the dependence on the beam polarisation. In $e^- p$ ($e^+ p$) scattering, the polarisation dependence is given by $1 + P_e$ ($1 - P_e$) for LQs coupling to right-handed fermions and $1 - P_e$ ($1 + P_e$) for LQs coupling to left-handed fermions.

The expected width of a LQ state with a mass between 100 and 300 GeV and a Yukawa coupling $\lambda = 0.1$ ranges from 0.01 to 0.2 GeV. This justifies the use of the NWA for the s-channel contribution. To simulate a LQ signal in the MC, the s-channel term was added to the interference terms and the DIS MC events were reweighted. To reduce statistical fluctuations, the prediction from the NWA was smeared with a Gaussian narrower than the experimental resolution before adding the interference terms.

The effect of QED initial-state radiation, which decreases the production cross section, was taken into account for both resonant and non-resonant LQ production. The effect is larger for resonant LQ production and ranges up to 25% for M_{LQ} close to $\sqrt{s}$.

The polarisation dependence is expected to be different for LQ production and DIS. The separation of the data according to polarisation therefore provides a handle to identify a possible LQ signal.

Another possibility to isolate a leptoquark signal is the angular dependence of the process. The variable θ^*, the lepton scattering angle in the lepton-jets centre-of-mass frame,

can be used to improve the signal-to-background ratio, especially for resonance production. The decay of a scalar resonance, for example, will result in a flat distribution in $\cos\theta^*$, while NC DIS events show approximately a $1/(1-\cos\theta^*)^2$ distribution.

5 Signal search

Events from a hypothetical resonance decaying into eq (νq) have a topology identical to DIS NC (CC) events. Hence the final state from a high-mass resonance is expected to have at least one jet and either an identified final-state electron or large missing transverse momentum. The lepton-jet invariant mass was calculated as

$$M_{ljs} = \sqrt{E_{ljs}^2 - \vec{p}_{ljs}^{\,2}}, \tag{1}$$

where E_{ljs} is the sum of the energies of the outgoing lepton and the selected jets and $\vec{p}_{ljs}$ is the vector sum of the lepton and jets momenta. The modulus of the transverse momentum, p_T, and the net transverse energy, E_T, are defined as

$$\begin{aligned} p_T^2 = \; & p_X^2 + p_Y^2 = \left(\sum_i E_i \sin\theta_i \cos\phi_i\right)^2 + \left(\sum_i E_i \sin\theta_i \sin\phi_i\right)^2, \\ E_T = & \sum_i E_i \sin\theta_i, \end{aligned} \tag{2}$$

where the sum runs over all calorimeter energy deposits, E_i. The polar and azimuthal angles, θ_i and ϕ_i, of the calorimeter energy deposits were measured relative to the reconstructed event vertex. The quantity $E - p_Z$, also used in the event selection, is defined as

$$E - p_Z \equiv \sum_i (E - p_Z)_i = \sum_i (E_i - E_i \cos\theta_i). \tag{3}$$

The hadronic polar angle was calculated as [33]

$$\cos\gamma_h = \frac{P_{T,\mathrm{had}}^2 - (E - P_Z)_{\mathrm{had}}}{P_{T,\mathrm{had}}^2 + (E - P_Z)_{\mathrm{had}}}, \tag{4}$$

where $P_{T,\mathrm{had}}^2$ and $(E - P_Z)_{\mathrm{had}}$ are calculated as in Equations (2) and (3), but with the sum running only over the calorimeter energy deposits belonging to the hadronic final state. In case of the CC topology, $P_{T,\mathrm{had}}^2$ and $(E - P_Z)_{\mathrm{had}}$ are equivalent to p_T^2 and $E - p_Z$ from Equations (2) and (3), respectively.

5.1 Neutral current, $ep \to eX$, topology

Event selection

The double-angle (DA) method [34] was used to reconstruct the kinematic variables. In this method, the polar angle of the scattered electron and the hadronic polar angle (see Eq. (4)) were used to reconstruct the kinematic variables $x_{\rm DA}$, $y_{\rm DA}$, and $Q^2_{\rm DA}$. The inelasticity y was also reconstructed as y_e, using the electron method [34].

Events with the topology $ep \to eX$, where X denotes one or more jets, were selected using the following criteria:

- the Z coordinate of the reconstructed event vertex was required to be in the range $|Z| < 30$ cm, consistent with an ep collision;
- an electron identified in the CAL [35] was required. If the electron was found within the acceptance of the tracking detectors, a track matched to the energy deposit in the calorimeter was required with the distance of closest approach between the track extrapolated to the calorimeter surface and the energy cluster position to be less than 10 cm and the electron track momentum, $p_e^{\rm trk}$, to be larger than 3 GeV. A matched track was not required if the electron emerged at a polar angle outside the acceptance of the tracking detector. Instead the electron was required to have a transverse momentum greater than 30 GeV. An isolation requirement was imposed such that the energy not associated with the electron in an $\eta - \phi$ cone of radius 0.8 centred on the electron was less than 5 GeV;
- a fiducial-volume cut was applied to the electron to guarantee that the experimental acceptance was well understood. It excluded the transition regions between the FCAL and the BCAL. It also excluded the regions within 1.5 cm of the module gaps in the BCAL;
- at least one hadronic jet with transverse momentum $p_T^j > 15$ GeV and $|\eta| < 3$, obtained using the k_T cluster algorithm [36] in its longitudinally invariant inclusive mode [37], was required. The centroid of any jet at the FCAL face was required to be outside a box of 40×40 cm^2 centred on the proton beam [38], in order to ensure good energy containment and to reduce the systematic uncertainties due to the proton remnant. Additional jets were required to have $p_T^j > 10$ GeV and $|\eta| < 3$;
- to restrict the phase space to the region most relevant to the LQ search, cuts on $Q^2_{\rm DA} > 2500\,{\rm GeV}^2$ and $x_{\rm DA} > 0.1$ were applied. Higher values of x and Q^2 correspond to higher LQ masses, where the signal-to-background ratio for leptoquark events is higher;
- to avoid phase-space regions in which the DIS MC generator was not valid, the quantity $y_{\rm DA}(1 - x_{\rm DA})^2$ was required to be larger than 0.004;

- to remove background from photoproduction events and beam-gas events overlaid on NC events, the requirements $38 < E - p_Z < 65\,\text{GeV}$ and $y_e < 0.95$ were imposed. To remove cosmic-ray events and beam-related background events, the quantity $p_T/\sqrt{E_T}$ was required to be less than $4\sqrt{\text{GeV}}$ and the quantity p_T/E_T was required to be less than 0.7. Elastic QED Compton events were rejected by considering the balance between the photon and the electron [39].

The mass shifts and resolutions for resonant lepton-quark states were calculated from the LQ MC. The mass resolution, determined from a Gaussian fit to the peak of the reconstructed mass spectrum, fell from 5% to 3% as the resonant mass increased from 150 to 290 GeV. Any mass shift was within 0.5% for LQ masses between 150 and 290 GeV.

Search results

After the above selection, 9 369 events were found in the data from 2003–2007, compared to 9 465 ± 494 expected from the NC MC and the evaluation of its systematic uncertainties (see below). The measured distributions of the M_{ejs} spectra for e^-p (e^+p) data with a left-handed and a right-handed lepton beam are shown in Figs. 2 and 3 (Figs. 4 and 5), respectively. A cut on $\cos\theta^* < 0.4$, introduced to suppress further the SM background [2, 3], was also applied. The upper parts of the plots show the spectra with and without the $\cos\theta^*$ cut, while the lower parts show the ratio of the observed spectrum to SM expectations with no cut applied on $\cos\theta^*$. Good agreement is seen between the data and the SM NC prediction. Figures 6 and 7 show the e^-p data for the left-handed electron beam together with the predictions for a S_0^L LQ state with a mass of 210 GeV and a coupling λ of 0.3 as well as a mass of 400 GeV and a coupling λ of 1 without and with a $\cos\theta^*$ cut, respectively.

Systematic uncertainties

The uncertainty on the expected number of events from SM NC DIS processes was investigated. Relevant were [33]:

- the uncertainty on the calorimeter energy scale, 1% for electrons and 2% for hadrons. This led to an uncertainty of 1% (6%) in the NC expectation for M_{ejs}=150 (220) GeV;
- the uncertainty on the parton densities as estimated by Botje [40], which gave an uncertainty of 3% (5%) in the NC expectation for M_{ejs}=150 (220) GeV;
- the uncertainty on the luminosity determination of 1.8% for electron and 2.2% for positron beams[4], which is directly reflected in the result.

[4]For a fraction of the positron data, the uncertainty was 3.5%, while for most of the positron data the uncertainty was 1.8%. This lead to a total uncertainty of 2.2%.

The overall systematic uncertainties on the background expectations were obtained by adding all relevant contributions in quadrature. They are shown as hatched bands in Figs. 2, 3, 4 and 5. For a given mass, the systematic uncertainty for the LQ signal is assumed to be the same as for the SM background.

5.2 Charged current, $ep \to \nu X$, topology

Event selection

The events with the topology $ep \to \nu X$, where X denotes one or more jets, are classified according to γ_0, the hadronic polar angle (see Eq. (4)) assuming a nominal vertex position of $Z = 0$. Events for which the hadronic system is not contained in the CTD acceptance ($\gamma_0 \leq 0.4$ rad) are called low-γ_0 events. The hadronic systems of high-γ_0 events with $\gamma_0 > 0.4$ rad are inside the CTD acceptance, so that cuts based on tracking information can be applied. The kinematic variables were reconstructed using the Jacquet-Blondel method [41].

The events were selected using the following criteria:

- the Z coordinate of the reconstructed event vertex was required to be in the range $|Z| < 30$ cm, consistent with an ep collision;
- to restrict the phase space to the region most relevant to the LQ search, a cut on $Q^2_{\rm JB} > 700\,{\rm GeV}^2$ was applied. Since the resolution on $Q^2_{\rm JB}$ was poor at high y, a cut on $y_{\rm JB} < 0.9$ was added;
- a missing transverse momentum $p_T > 22\,{\rm GeV}$ was required and, to suppress beam-gas events, the missing transverse momentum excluding the calorimeter cells adjacent to the forward beam hole was required to exceed 20 GeV. Compared to the ZEUS CC DIS analyses [42–44], these cuts are more stringent because CC events with low p_T lead to low invariant masses of the LQs and are therefore not of interest in this analysis;
- in the high-γ_0 region, cuts based on the number and quality of tracks were applied. Tracks with a transverse momentum above 0.2 GeV were selected. They were required to start from the MVD or the innermost superlayer of the CTD, and had to reach at least the third superlayer of the CTD. If in addition they pointed to the primary vertex, they were considered as "good tracks". At least one good track was required in the event and the ratio of the total number of tracks to the number of good tracks had to fulfill the requirement $\frac{N_{\rm trk}-20}{N_{\rm gtrk}} < 4$, where $N_{\rm trk}$ is the total number of tracks and $N_{\rm gtrk}$ is the number of good tracks. This cut removed beam-gas events which are characterised by a high number of poor-quality tracks;

- at least one hadronic jet with transverse momentum $p_T^j > 10\,\text{GeV}$ and $|\eta| < 3$, obtained using the k_T cluster algorithm [36] in its longitudinally invariant inclusive mode [37], was required. The centroids of all jets at the FCAL face were required to be outside a box of 40×40 cm^2 centred on the proton beam [38], in order to ensure good energy containment and to reduce the systematic uncertainties due to the proton remnant.

- to reject photoproduction and di-lepton background, for events with $p_T < 30\,\text{GeV}$ a dedicated cut based on the energy distribution in the detector relative to the total transverse momentum was used. The transverse momentum sum for the calorimeter cells with a positive contribution to the total transverse momentum (parallel component V_P) and the corresponding sum for cells giving a negative contribution to the total transverse momentum (antiparallel component V_{AP}) had to satisfy the condition $V_{AP}/V_P < 0.35$ [44]. This requirement demanded an azimuthally collimated energy flow. In addition, for events with at least one good track, the azimuthal-angle difference, $\Delta\phi$, between the missing transverse momentum measured by the tracks[5] and that measured by the calorimeter was required to be less than 45° for events with $p_T < 30\,\text{GeV}$ and less than 60° otherwise. This cut rejects events caused by cosmic rays or muons in the beam halo as well as beam-gas events;

- NC events were removed by discarding events containing electron candidates with an energy greater than 4 GeV [43];

- requirements on energy fractions in the calorimeter cells plus muon-finding algorithms based on tracking, calorimeter and muon-chamber information were used to reject events caused by cosmic rays or muons in the beam halo. Furthermore, the deposition times of the energy clusters in the calorimeter were checked to be consistent with the bunch-crossing time to reject events due to interactions between the beams and residual gas in the beam pipe or upstream accelerator components. In addition, topological cuts on the transverse and longitudinal shower shape were imposed to reject beam-halo muon events that produced a shower inside the FCAL. Cuts on the calorimeter cell with the highest transverse energy were applied to reject sparks faking a CC event [33].

The neutrino energy and angle were calculated by assuming that missing p_T and missing $E - P_Z$ were carried away by a single neutrino and used to calculate the invariant mass of the ν-jets system, $M_{\nu js}$, according to Eq. (1).

The shift and resolution of the invariant mass were studied by using the LQ MC events and fitting the mass peak with a Gaussian function. The resulting mass shift was within 0.5% for LQ masses between 150 and 290 GeV, with the resolution varying from 8% to 6%, respectively.

[5]The missing transverse momentum measured by the tracks is calculated using all the good tracks.

Search results

After the above selection, 8 990 events were found in the data from 2003–2007, compared to 9 068 $\pm$ 501 expected from the CC MC and the evaluation of its systematic uncertainties (see below). The measured distributions of the $M_{\nu js}$ spectra for the left-handed and right-handed e^-p (e^+p) data are shown in Figs. 8 and 9 (Figs. 10 and 11). The upper parts of the plots show the spectra with and without the cut $\cos\theta^* < 0.4$, while the lower parts show the ratio of the observed spectrum to SM expectations with no cut applied on $\cos\theta^*$. Good agreement is seen between the data and the SM CC prediction.

Systematic uncertainties

The uncertainty on the predicted background from SM CC DIS processes was investigated. The uncertainties found to be relevant [33] are similar to those described in Section 5.1 for the $ep \to eX$ case and arise from:

- the uncertainy on the hadronic energy scale of 2%, which led to an uncertainty of 3% (10%) in the CC expectation for $M_{\nu js}$=150 (220) GeV;
- the uncertainty on the parton densities as estimated by Botje [40], giving 3% (4%) and 7% (9%) uncertainties on the cross section for e^-p and e^+p, respectively, for $M_{\nu js}$=150 (220) GeV. The correlations between e^-p and e^+p as well as NC and CC cross section uncertainties were taken into account;
- the uncertainty on the luminosity determination of 1.8% for electron and 2.2% for positron beams, which is directly reflected in the result;
- the uncertainty on the measured polarisation of 4.2%. To be conservative, the TPOL uncertainty, which is larger than the LPOL uncertainty, was used. This led to an uncertainty on the SM cross section of 0.9% (2.4%) for left-handed e^-p (e^+p) data and 1.8% (1.0%) for right-handed e^-p (e^+p) data, respectively.

The overall systematic uncertainties on the background expectations were obtained by adding all relevant contributions in quadrature. They are shown as hatched bands in Figs. 8, 9, 10 and 11. For a given mass, the systematic uncertainty for the LQ signal is assumed to be the same as for the SM background.

6 Limits on leptoquarks

The expectation from a potential LQ signal was obtained by reweighting the DIS MC according to the cross sections predicted in the BRW model (see Section 4). Each MC

event is reweighted with the following weighting factor, WF:

$$\mathrm{WF}(x,y;P_e;M_{\mathrm{LQ}},\lambda)\frac{\frac{d^2\sigma^{\mathrm{SM}+LQ}}{dxdy}(x,y;P_e;M_{\mathrm{LQ}},\lambda)}{\frac{d^2\sigma^{\mathrm{SM}}}{dxdy}(x,y;P_e)},$$

where x and y are the true kinematic variables of the MC simulation, and P_e is the average polarisation of the data sample given in Table 1. The effect of QED initial-state radiation was taken into account.

The limits were calculated including the results of the search presented here and the data recorded with the ZEUS detector in the years 1994–2000 [4]. They were set using a binned likelihood technique in the $(M_{ljs}, \cos\theta^*)$ plane. The region $150 < M_{ljs} < 320\,\mathrm{GeV}$ was used. The data were binned separately for each of the data sets listed in Table 1, thereby taking into account different beam charges and polarisation. For leptoquark states with νq decays, both the $eq \to eX$ and the $eq \to \nu X$ samples were used, while for leptoquark states decaying only to eq, only the $eq \to eX$ samples were used.

The upper limit on the coupling strength, λ_{limit}, as a function of M_{LQ}, was obtained by solving

$$\int_0^{\lambda^2_{\mathrm{limit}}} d\lambda^2 L(M_{\mathrm{LQ}},\lambda) = 0.95 \int_0^{\infty} d\lambda^2 L(M_{\mathrm{LQ}},\lambda), \tag{5}$$

where L is the product of the Poisson probabilities of the observed number of events in bin i, N_i, with the expectation, μ_i, convoluted with Gaussian distributions for the main systematic uncertainties, yielding a modified expectation μ_i':

$$L = \int_{-\infty}^{\infty} \prod_j d\delta_j \frac{1}{\sqrt{2\pi}} e^{(-\delta_j^2/2)} \prod_i e^{(-\mu_i')} \frac{{\mu_i'}^{N_i}}{N_i!}.$$

The index j denotes the source of a systematic uncertainty and δ_j corresponds to the variation of the j^{th} systematic parameter in units of the nominal values quoted in Sections 5.1 and 5.2. The index i runs over the bins in M_{ljs}-$\cos\theta^*$ and the relevant data sets. The modified expectation was calculated as

$$\mu_i' = \mu_i \prod_j (1+\sigma_{ij})^{\delta_j},$$

where σ_{ij} gives the fractional variation of μ_i under the nominal shift in the j^{th} systematic parameter. This *ansatz* of μ_i' reduces to a linear dependence of μ_i' on each δ_j when δ_j is small, while avoiding the possibility of μ_i' becoming negative which would arise if μ_i' was defined as a linear function of the δ_j.

The coupling limits for the 14 BRW LQs listed in Table 2 were calculated for masses up to 1 TeV. For large LQ masses, i.e. $M_{\mathrm{LQ}} \gg \sqrt{s}$, their exchange can be described as

a contact interaction with an effective coupling proportional to $\lambda^2/M_{\rm LQ}^2$. Table 3 shows the limits on λ for all BRW LQs at $M_{\rm LQ} = 1\,\text{TeV}$.

Figures 12–15 show the coupling limits on the scalar and vector LQs with $F = 0$ and $F = 2$, respectively, where $F = 3B + L$ is the fermion number of the LQ and B and L are the baryon and lepton numbers, respectively. The limits range from 0.004–0.017 for $M_{\rm LQ} = 150\,\text{GeV}$, and from 0.43–3.24 for $M_{\rm LQ} = 1\,\text{TeV}$. The lowest masses for which LQs with $\lambda = 0.1$ and with $\lambda = 0.3$ are not excluded are summarised in Table 4. They range from 274 to 300 GeV for $\lambda = 0.1$ and from 290 to 699 GeV for $\lambda = 0.3$.

The limit on the LQ state $\tilde{S}^L_{1/2}$ (S^L_0) can be interpreted as a limit on $\lambda\sqrt{\beta}$ for an up-type squark $\tilde{u}_L$ (a down-type squark $\tilde{d}_R$) in supersymmetric models with R-parity violation [45], where λ is the coupling of $\tilde{u}_L$ to eq ($\tilde{d}_R$ to eq and νq) and β is the branching fraction of the squarks to lepton (e or ν) and quark[6].

Figure 16 (17) shows the limits on the $S^L_{1/2}$ (S^L_1) LQ compared to the limits from ATLAS [10], H1 [5] L3 [6] and OPAL [7]. The L3 and OPAL limits were evaluated up to 500 GeV. Limits using pp or $p\bar{p}$ collisions are obtained from leptoquark pair production, which is independent of λ. Therefore it is not obvious whether the limits should be compared directly. The ATLAS exclusion range given in Fig. 17 also depends on the assumption that the branching ratio of the LQ state to electron and quark is one. Limits using e^+e^- collisions are obtained from a search for indirect effects in the process $e^+e^- \to q\bar{q}$. In general, the limits from this analysis are significantly better than the LEP limits for $M_{\rm LQ} < \sqrt{s}$, and comparable for $M_{\rm LQ} > \sqrt{s}$. The limits obtained by ZEUS are similar to those obtained by H1.

7 Conclusions

Data recorded by the ZEUS experiment at HERA were used to search for the presence of first-generation scalar and vector leptoquarks. The data samples include 185 pb^{-1} of e^-p and 181 pb^{-1} of e^+p collisions with polarised electrons and positrons. No resonances or other deviations from the Standard Model were found. The inclusion of data with unpolarised beams yields a total set of data corresponding to 498 pb^{-1}, which was used to set upper limits on the Yukawa coupling λ for the 14 Buchmüller-Rückl-Wyler leptoquark states as a function of the leptoquark mass. Assuming $\lambda = 0.3$, the mass limits range from 290 to 699 GeV.

[6] The branching fractions of the squarks to eq and νq are assumed to be $\beta_{eq} = \beta,\ \beta_{\nu q} = 0$ for $\tilde{u}_L$, and $\beta_{eq} = 0.5\,\beta,\ \beta_{\nu q} = 0.5\,\beta$ for $\tilde{d}_R$.

Acknowledgments

We appreciate the contributions to the construction and maintenance of the ZEUS detector of many people who are not listed as authors. The HERA machine group and the DESY computing staff are especially acknowledged for their success in providing excellent operation of the collider and the data-analysis environment. We thank the DESY directorate for their strong support and encouragement.

References

[1] W. Buchmüller, R. Rückl and D. Wyler, Phys. Lett. **B 191**, 442 (1987). Erratum in Phys. Lett. **B 448**, 320 (1999).

[2] ZEUS Coll., J. Breitweg et al., Eur. Phys. J. **C 16**, 253 (2000).

[3] ZEUS Coll., J. Breitweg et al., Phys. Rev. **D 63**, 052002 (2001).

[4] ZEUS Coll., S. Chekanov et al., Phys. Rev. **D 68**, 052004 (2003).

[5] H1 Coll., F.D. Aaron et al., Phys. Lett. **B 704**, 388 (2011).

[6] L3 Coll., M. Acciarri et al., Phys. Lett. **B 489**, 81 (2000).

[7] OPAL Coll., G. Abbiendi et al., Eur. Phys. J. **C 6**, 1 (1999).

[8] D0 Coll., V.M. Abazov et al., Phys. Lett. **B 681**, 224 (2009).

[9] CDF Coll., D. Acosta et al., Phys. Rev. **D 72**, 051107 (2005).

[10] ATLAS Coll., G. Aad et al., Phys. Lett. **B 709**, 158 (2012).

[11] CMS Coll., V. Khachatryan et al., Phys. Rev. Lett. **106**, 201802 (2011).

[12] CMS Coll., S. Chatrchyan et al., Phys. Lett. **B 703**, 246 (2011).

[13] CTEQ Coll., H.L. Lai et al., Eur. Phys. J. **C 12**, 375 (2000).

[14] ZEUS Coll., U. Holm (ed.), *The ZEUS Detector*. Status Report (unpublished), DESY (1993), available on `http://www-zeus.desy.de/bluebook/bluebook.html`.

[15] N. Harnew et al., Nucl. Inst. Meth. **A 279**, 290 (1989);
B. Foster et al., Nucl. Phys. Proc. Suppl. **B 32**, 181 (1993);
B. Foster et al., Nucl. Inst. Meth. **A 338**, 254 (1994).

[16] A. Polini et al., Nucl. Inst. Meth. **A 581**, 656 (2007).

[17] M. Derrick et al., Nucl. Inst. Meth. **A 309**, 77 (1991);
A. Andresen et al., Nucl. Inst. Meth. **A 309**, 101 (1991);
A. Caldwell et al., Nucl. Inst. Meth. **A 321**, 356 (1992);
A. Bernstein et al., Nucl. Inst. Meth. **A 336**, 23 (1993).

[18] J. Andruszków et al., Preprint DESY-92-066, DESY, 1992;
ZEUS Coll., M. Derrick et al., Z. Phys. **C 63**, 391 (1994);
J. Andruszków et al., Acta Phys. Pol. **B 32**, 2025 (2001).

[19] M. Helbich et al., Nucl. Inst. Meth. **A 565**, 572 (2006).

[20] A.A. Sokolov and I.M. Ternov, Sov. Phys. Dokl. **8**, 1203 (1964).

[21] V.N. Baier and V.A. Khoze, Sov. J. Nucl. Phys. **9**, 238 (1969).

[22] D.P. Barber et al., Nucl. Inst. Meth. **A 329**, 79 (1993).

[23] M. Beckmann et al., Nucl. Inst. Meth. **A 479**, 334 (2002).

[24] A. Kwiatkowski, H. Spiesberger and H.-J. Möhring, Comp. Phys. Comm. **69**, 155 (1992). Also in *Proc. Workshop Physics at HERA*, eds. W. Buchmüller and G.Ingelman, (DESY, Hamburg, 1991);
H. Spiesberger, *An Event Generator for ep Interactions at HERA Including Radiative Processes (Version 4.6)*, 1996, available on `http://www.desy.de/~hspiesb/heracles.html`.

[25] H. Spiesberger, HERACLES *and* DJANGOH*: Event Generation for ep Interactions at HERA Including Radiative Processes*, 1998, available on `http://www.desy.de/~hspiesb/djangoh.html`.

[26] L. Lönnblad, Comp. Phys. Comm. **71**, 15 (1992).

[27] T. Sjöstrand, Comp. Phys. Comm. **39**, 347 (1986);
T. Sjöstrand and M. Bengtsson, Comp. Phys. Comm. **43**, 367 (1987);
T. Sjöstrand, Comp. Phys. Comm. **82**, 74 (1994).

[28] T. Sjöstrand et al., Comp. Phys. Comm. **135**, 238 (2001).

[29] C. Friberg, E. Norrbin and T. Sjöstrand, Phys. Lett. **B 403**, 329 (1997).

[30] R. Brun et al., GEANT3, Technical Report CERN-DD/EE/84-1, CERN, 1987.

[31] T. Plehn et al., Z. Phys. **C 74**, 611 (1997).

[32] Z. Kunszt and W.J. Stirling, Z. Phys. **C 75**, 453 (1997).

[33] A. Hüttmann. Ph.D. Thesis, Universität Hamburg, Germany, Report DESY-THESIS-2009-035, 2009.

[34] S. Bentvelsen, J. Engelen and P. Kooijman, *Proc. Workshop on Physics at HERA*, W. Buchmüller and G. Ingelman (eds.), Vol. 1, p. 23. Hamburg, Germany, DESY (1992);
K.C. Höger, *Proc. Workshop on Physics at HERA*, W. Buchmüller and G. Ingelman (eds.), Vol. 1, p. 43. Hamburg, Germany, DESY (1992).

[35] ZEUS Coll., J. Breitweg et al., Eur. Phys. J. **C 11**, 427 (1999).

[36] S. Catani et al., Nucl. Phys. **B 406**, 187 (1993).

[37] S.D. Ellis and D.E. Soper, Phys. Rev. **D 48**, 3160 (1993).

[38] Inderpal Singh. Ph.D. Thesis, Panjab University, India, 2011. Unpublished.

[39] Y.D. Ri. Ph.D. Thesis, Tokyo Metropolitan University, Japan, Report KEK-report 2009-2, 2009.

[40] M. Botje, Eur. Phys. J. **C 14**, 285 (2000).

[41] F. Jacquet and A. Blondel, *Proceedings of the Study for an ep Facility for Europe*, U. Amaldi (ed.), p. 391. Hamburg, Germany (1979). Also in preprint DESY 79/48.

[42] ZEUS Coll., S. Chekanov et al., Phys. Lett. **B 637**, 210 (2006).

[43] ZEUS Coll., S. Chekanov et al., Eur. Phys. J. **C 61**, 223 (2009).

[44] ZEUS Coll., H. Abramowicz et al., Eur. Phys. J. **C 70**, 945 (2010).

[45] J. Butterworth and H. Dreiner, Nucl. Phys. **B 397**, 3 (1993).

[46] A. Djouadi et al., Z. Phys. **C 46**, 679 (1990).

period	lepton	luminosity (pb^{-1})	$\langle P_e \rangle$	$\sqrt{s}$ (GeV)
04–06	e^-	106	–0.27	318
04–06	e^-	79	0.30	318
03–04	e^+	17	–0.37	318
06–07		60		
03–04	e^+	21	0.32	318
06–07		83		
94–97	e^+	49	0	300
98–99	e^-	17	0	318
99–00	e^+	66	0	318

Table 1: *Details, including longitudinal polarisation, P_e, of the different data samples used.*

LQ species	charge	production	decay	branching ratio	coupling
F=0					
$S^L_{1/2}$	5/3	$e^+_R u_R$	e^+u	1	λ_L
$S^R_{1/2}$	5/3	$e^+_L u_L$	e^+u	1	λ_R
	2/3	$e^+_L d_L$	e^+d	1	$-\lambda_R$
$\tilde{S}^L_{1/2}$	-2/3	$e^+_R d_R$	e^+d	1	λ_L
V^L_0	2/3	$e^+_R d_L$	e^+d	1/2	λ_L
			$\bar{\nu}_e u$	1/2	λ_L
V^R_0	2/3	$e^+_L d_R$	e^+d	1	λ_R
$\tilde{V}^R_0$	5/3	$e^+_L u_R$	e^+u	1	λ_R
V^L_1	5/3	$e^+_R u_L$	e^+u	1	$\sqrt{2}\lambda_L$
	2/3	$e^+_R d_L$	e^+d	1/2	$-\lambda_L$
			$\bar{\nu}_e u$	1/2	λ_L
F=2					
S^L_0	–1/3	$e^-_L u_L$	e^-u	1/2	λ_L
			$\nu_e d$	1/2	$-\lambda_L$
S^R_0	–1/3	$e^-_R u_R$	e^-u	1	λ_R
$\tilde{S}^R_0$	–4/3	$e^-_R d_R$	e^-d	1	λ_R
S^L_1	–1/3	$e^-_L u_L$	e^-u	1/2	$-\lambda_L$
			$\nu_e d$	1/2	$-\lambda_L$
	–4/3	$e^-_L d_L$	e^-d	1	$-\sqrt{2}\lambda_L$
$V^L_{1/2}$	–4/3	$e^-_L d_R$	e^-d	1	λ_L
$V^R_{1/2}$	–4/3	$e^-_R d_L$	e^-d	1	λ_R
	–1/3	$e^-_R u_L$	e^-u	1	λ_R
$\tilde{V}^L_{1/2}$	–1/3	$e^-_L u_R$	e^-u	1	λ_L

Table 2: *Leptoquark species for fermion number $F = 0$ and $F = 2$ as defined in the Buchmüller-Rückl-Wyler model [1] and the corresponding couplings. Those LQs that couple only to neutrinos and quarks and therefore could not be produced at HERA are not listed. The LQ species are classified according to their spin (S for scalar and V for vector), their chirality (L or R) and their weak isospin ($0, 1/2, 1$). The leptoquarks $\tilde{S}$ and $\tilde{V}$ differ by two units of hypercharge from S and V, respectively. In addition, the electric charge of the leptoquarks, the production channel, as well as their allowed decay channels assuming lepton-flavour conservation are displayed. The nomenclature follows the Aachen convention [46].*

LQ type (F=0)	V_0^L	V_0^R	$\tilde{V}_0^R$	V_1^L	$S_{1/2}^L$	$S_{1/2}^R$	$\tilde{S}_{1/2}^L$
$\lambda_{\rm limit}$	0.87	1.91	0.76	0.43	1.00	2.29	1.91
LQ type (F=2)	S_0^L	S_0^R	$\tilde{S}_0^R$	S_1^L	$V_{1/2}^L$	$V_{1/2}^R$	$\tilde{V}_{1/2}^L$
$\lambda_{\rm limit}$	1.15	1.48	3.24	0.60	1.95	0.95	0.76

Table 3: *Upper limit on the Yukawa coupling, $\lambda_{\rm limit}$ as defined in Eq. (5), for the 14 BRW LQs at $M_{\rm LQ} = 1$ TeV.*

LQ type (F=0)	V_0^L	V_0^R	$\tilde{V}_0^R$	V_1^L	$S_{1/2}^L$	$S_{1/2}^R$	$\tilde{S}_{1/2}^L$
$M_{\rm LQ}$(GeV) ($\lambda_{\rm limit} = 0.1$)	276	275	295	300	295	294	274
$M_{\rm LQ}$(GeV) ($\lambda_{\rm limit} = 0.3$)	325	292	376	699	345	300	292
LQ type (F=2)	S_0^L	S_0^R	$\tilde{S}_0^R$	S_1^L	$V_{1/2}^L$	$V_{1/2}^R$	$\tilde{V}_{1/2}^L$
$M_{\rm LQ}$(GeV) ($\lambda_{\rm limit} = 0.1$)	295	292	274	298	278	293	293
$M_{\rm LQ}$(GeV) ($\lambda_{\rm limit} = 0.3$)	332	304	290	506	292	303	376

Table 4: *Lower limit for the masses of the 14 BRW LQs for $\lambda_{\rm limit}$=0.1 and $\lambda_{\rm limit}$=0.3 as deduced from Eq. (5).*

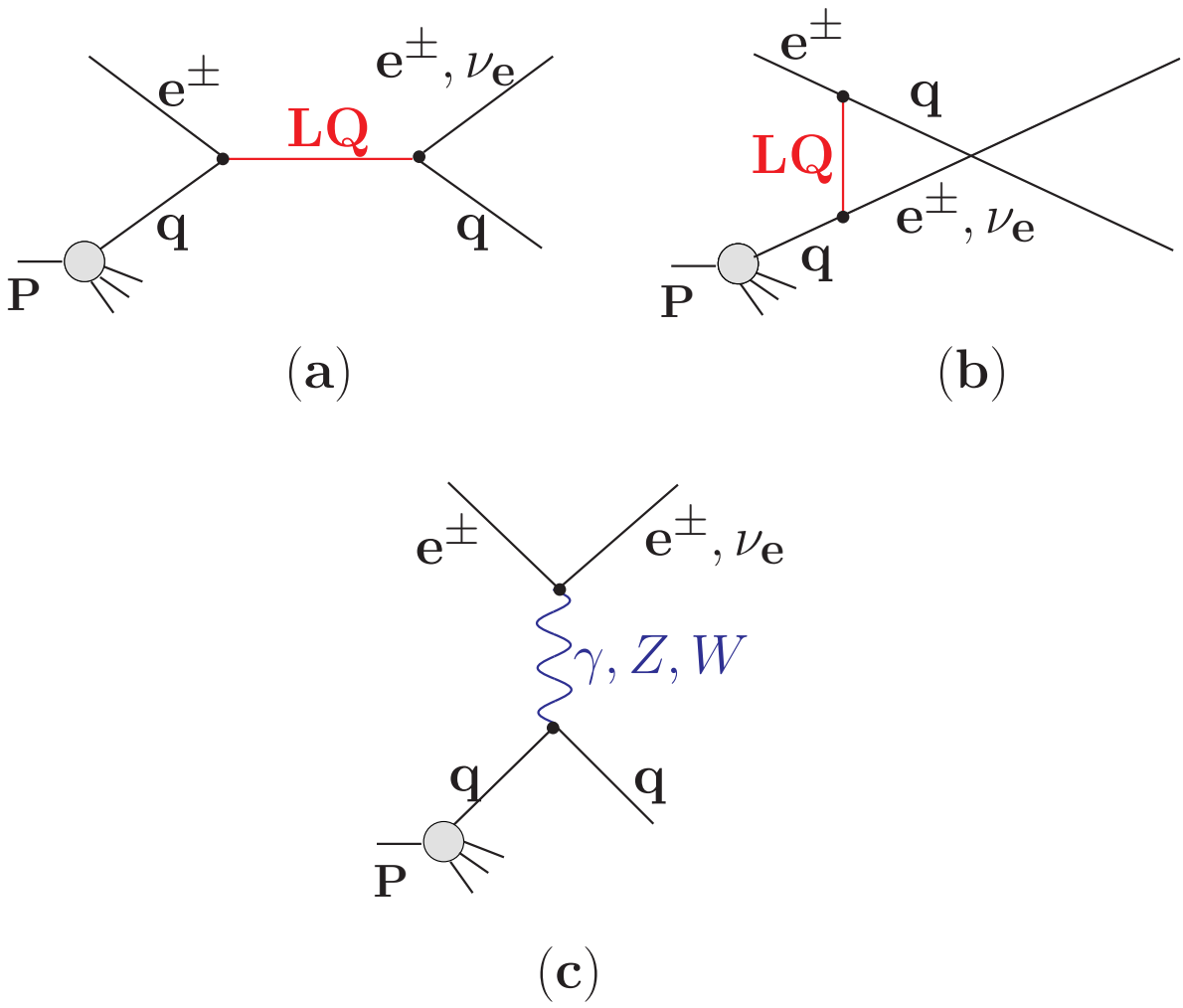

Figure 1: *Diagrams for (a) s-channel LQ production/exchange and (b) u-channel LQ exchange and for (c) SM deep inelastic scattering via photon, Z^0 and W exchange.*

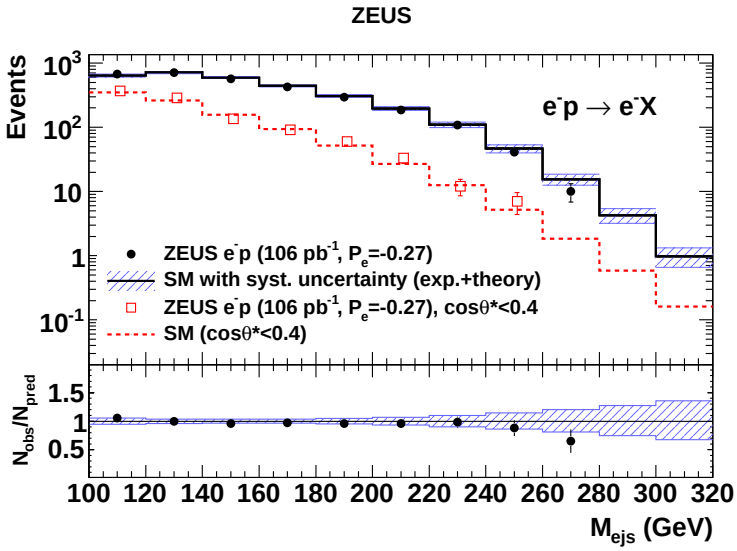

Figure 2: *Comparison of the left-handed e^-p sample (dots) and the NC SM expectation (solid histogram) for the reconstructed invariant mass, M_{ejs}, in the $e^-p \to e^-X$ topology. The data (open squares) and the SM expectation (dashed histogram) for $\cos\theta^* < 0.4$ are also shown. The shaded area shows the overall uncertainty of the SM MC expectation. The lower part of the plot shows the ratio between the data and the SM expectation without the $\cos\theta^*$ cut.*

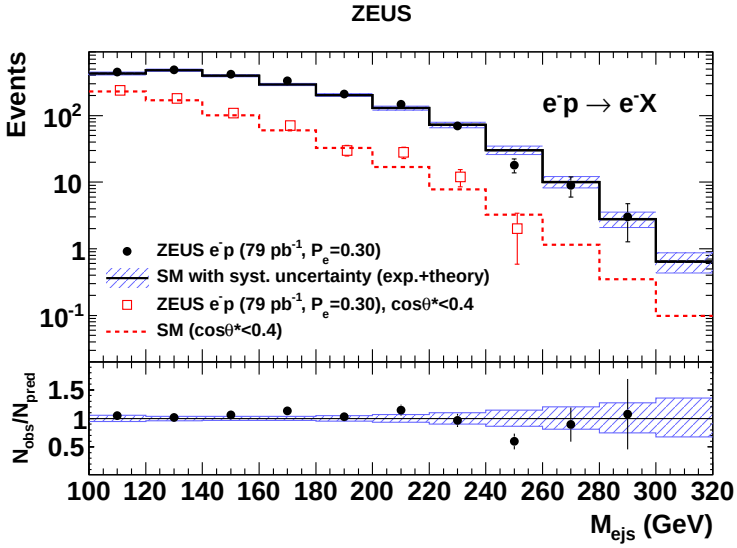

Figure 3: *Comparison of the right-handed e^-p sample (dots) and the NC SM expectation (solid histogram) for the reconstructed invariant mass, M_{ejs}, in the $e^-p \to e^-X$ topology. Other details as in the caption to Fig. 2.*

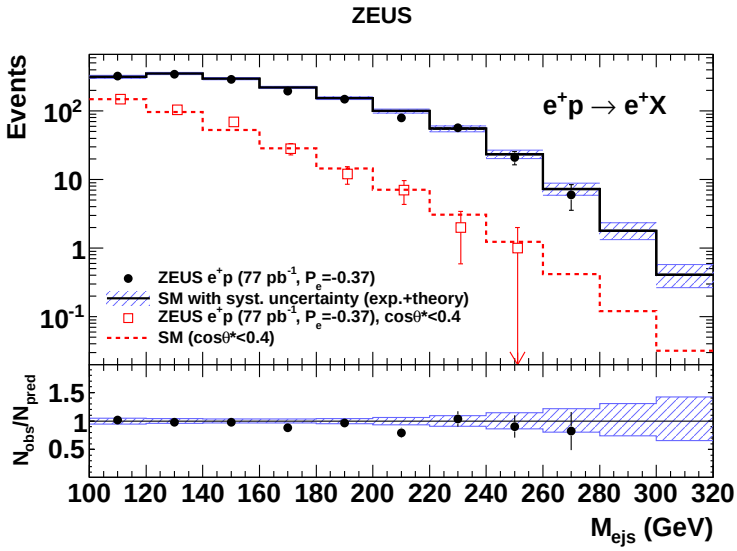

Figure 4: *Comparison of the left-handed e^+p sample (dots) and the NC SM expectation (solid histogram) for the reconstructed invariant mass, M_{ejs}, in the $e^+p \to e^+X$ topology. Other details as in the caption to Fig. 2.*

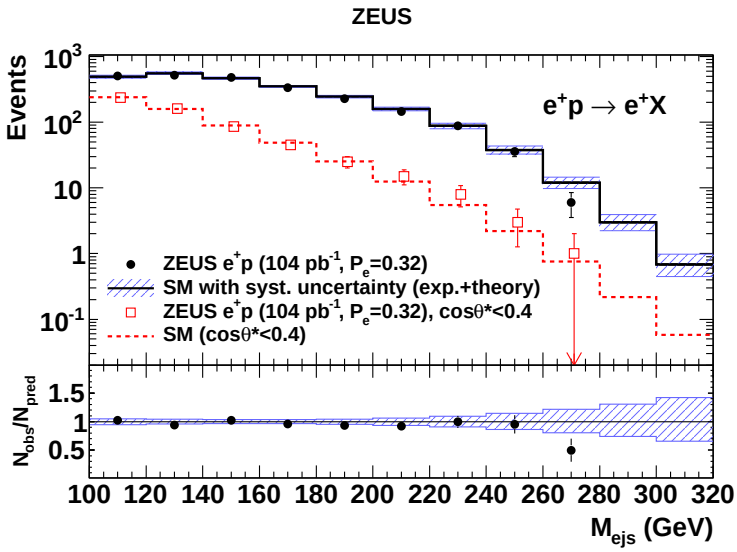

Figure 5: *Comparison of the right-handed e^+p sample (dots) and the NC SM expectation (solid histogram) for the reconstructed invariant mass, M_{ejs}, in the $e^+p \to e^+X$ topology. Other details as in the caption to Fig. 2.*

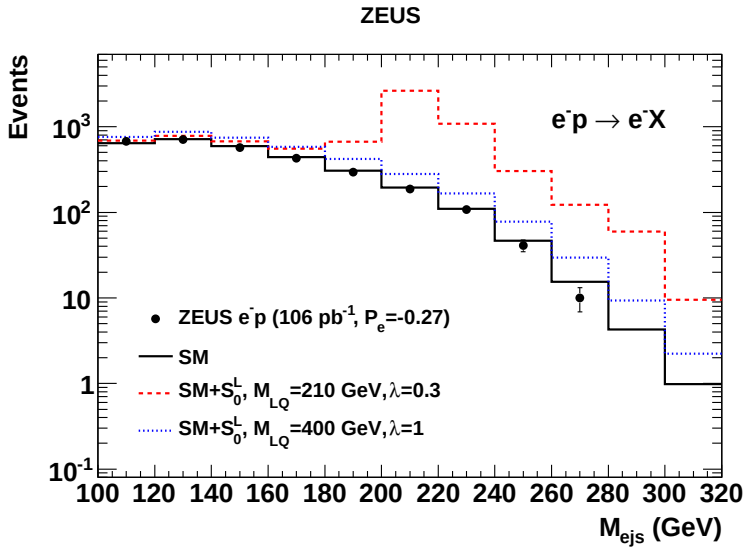

Figure 6: *Comparison of the reconstructed invariant mass, M_{ejs}, distribution in the $e^-p \to e^-X$ topology for the left-handed e^-p sample (dots) to the NC SM expectation (solid histogram) and to the predictions of the model including a S_0^L LQ state with a mass of 210 GeV and a coupling λ of 0.3 (dashed histogram) as well as a mass of 400 GeV and a coupling λ of 1 (dotted histogram).*

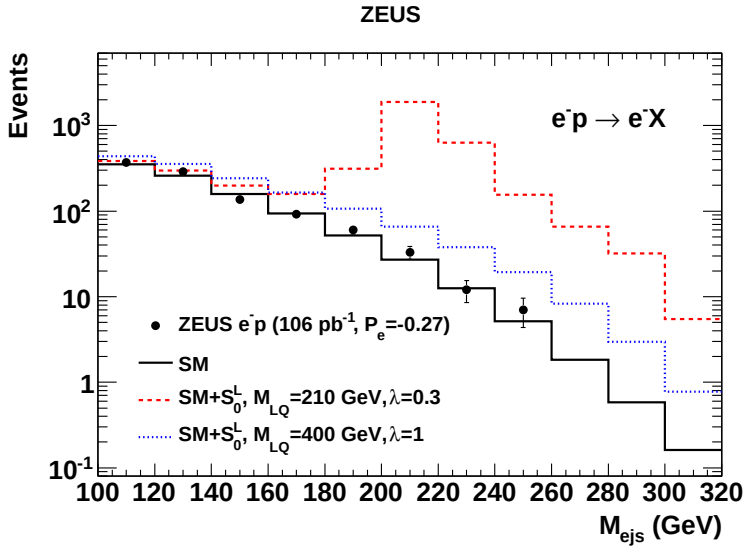

Figure 7: *As Fig. 6, but the cut on $\cos\theta^* < 0.4$ was applied.*

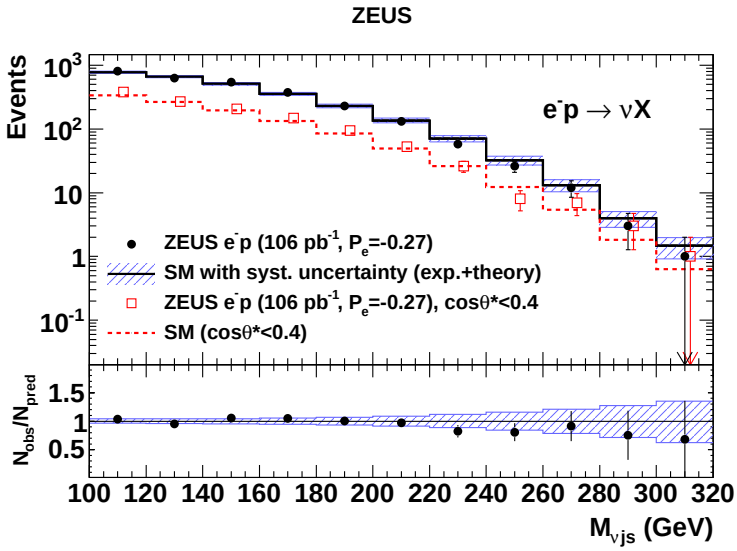

Figure 8: *Comparison of the left-handed e^-p sample (dots) and the CC SM expectation (solid histogram) for the reconstructed invariant mass, $M_{\nu js}$, in the $e^-p \to \nu X$ topology. The data (open squares) and the SM expectation (dashed histogram) for $\cos\theta^* < 0.4$ are also shown. The shaded area shows the overall uncertainty of the SM MC expectation. The lower part of the plot shows the ratio between the data and the SM expectation without the $\cos\theta^*$ cut.*

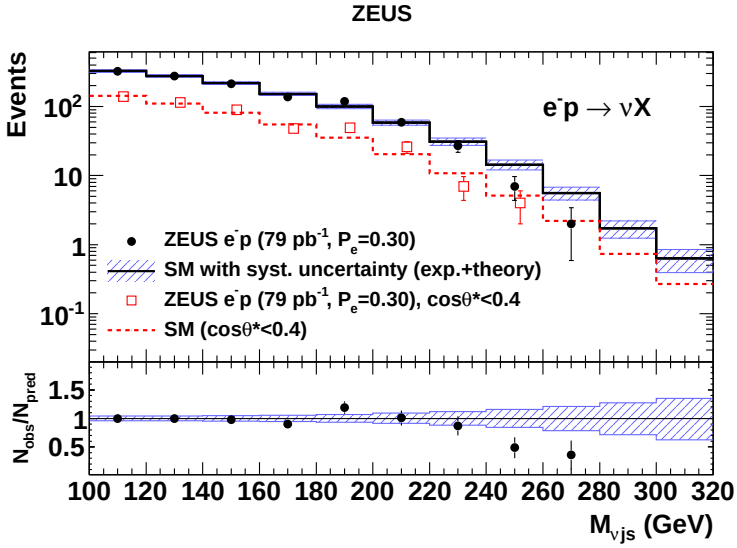

Figure 9: *Comparison of the right-handed e^-p sample (dots) and the CC SM expectation (solid histogram) for the reconstructed invariant mass, $M_{\nu js}$, in the $e^-p \to \nu X$ topology. Other details as in the caption to Fig. 8.*

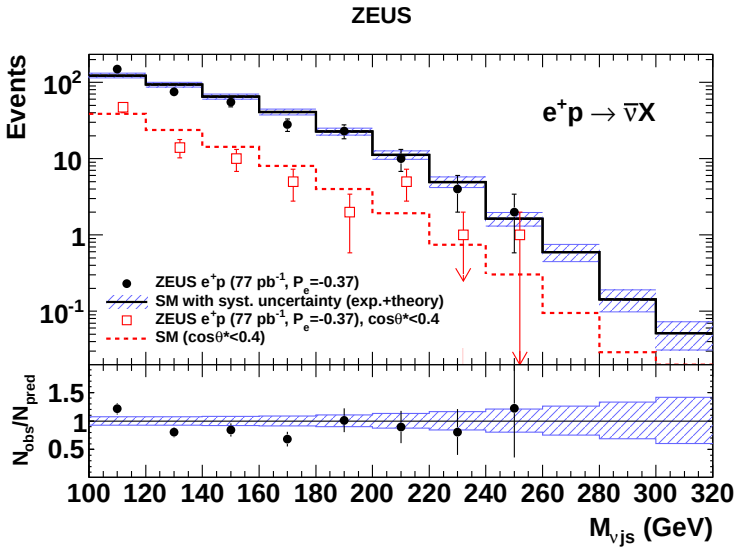

Figure 10: *Comparison of the left-handed e^+p sample (dots) and the CC SM expectation (solid histogram) for the reconstructed invariant mass, $M_{\nu js}$, in the $e^+p \to \bar{\nu}X$ topology. Other details as in the caption to Fig. 8.*

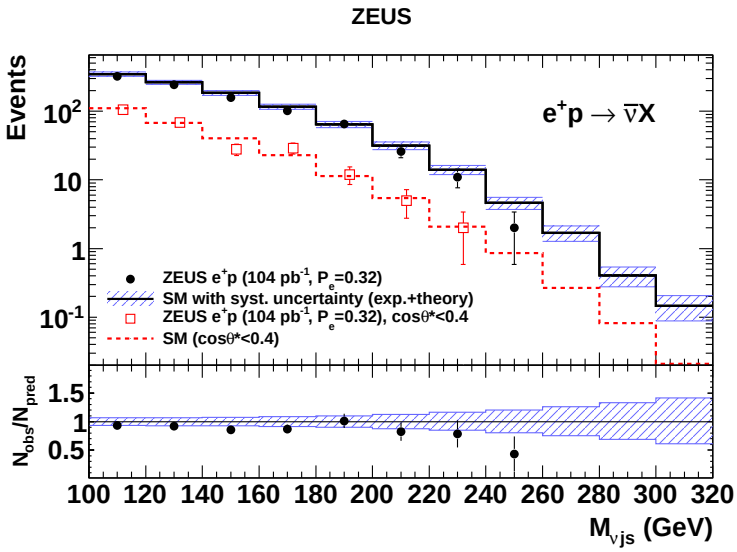

Figure 11: *Comparison of the right-handed e^+p sample (dots) and the CC SM expectation (solid histogram) for the reconstructed invariant mass, $M_{\nu js}$, in the $e^+p \to \bar{\nu}X$ topology. Other details as in the caption to Fig. 8.*

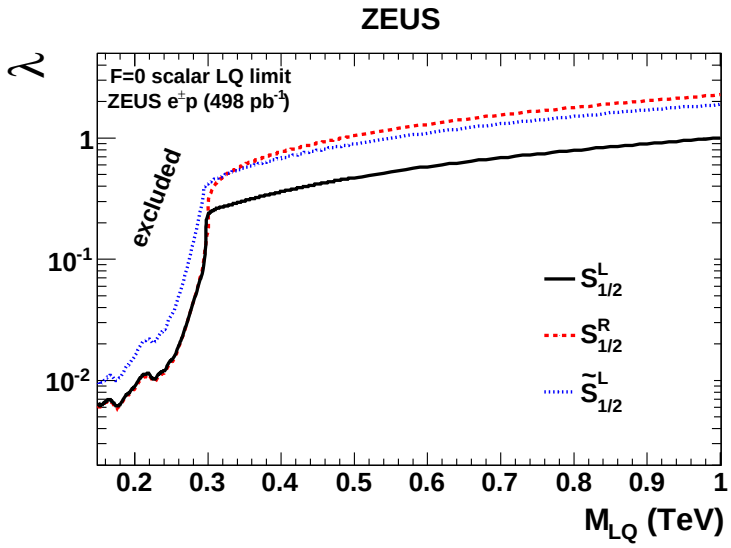

Figure 12: *Coupling limits, λ_{limit}, as a function of LQ mass for scalar F=0 BRW LQs. The areas above the curves are excluded according to Eq. (5).*

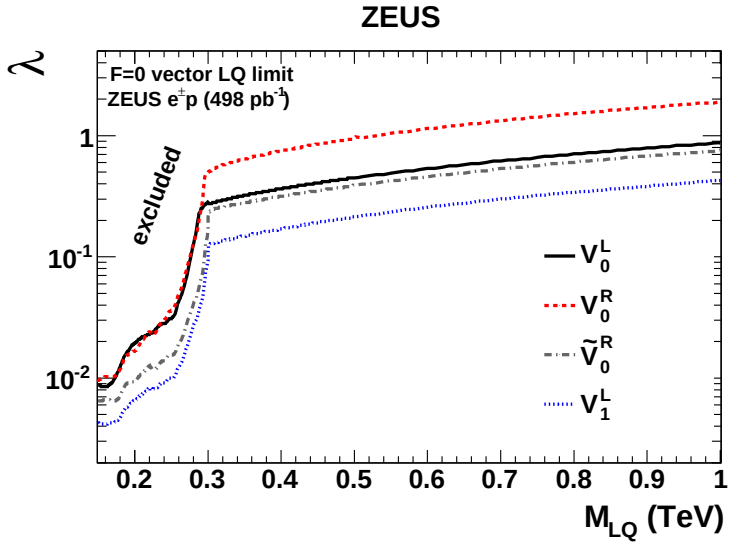

Figure 13: *Coupling limits, λ_{limit}, as a function of LQ mass for vector F=0 BRW LQs. The areas above the curves are excluded according to Eq. (5).*

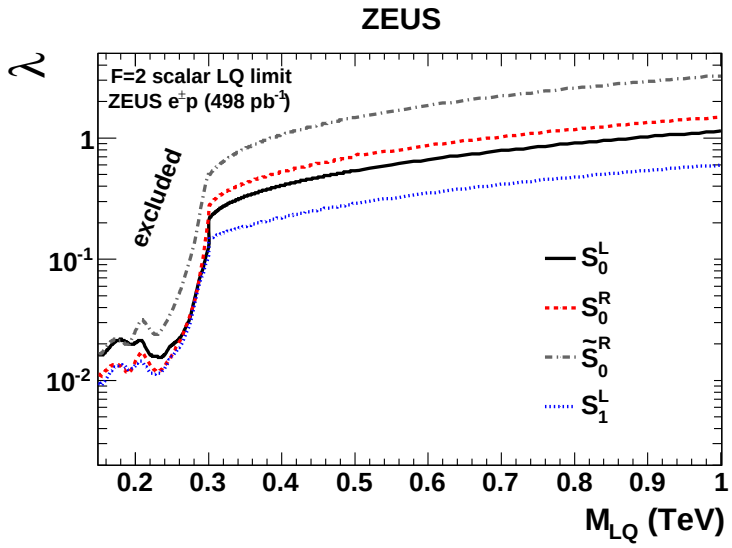

Figure 14: *Coupling limits, $\lambda_{\rm limit}$, as a function of LQ mass for scalar F=2 BRW LQs. The areas above the curves are excluded according to Eq. (5).*

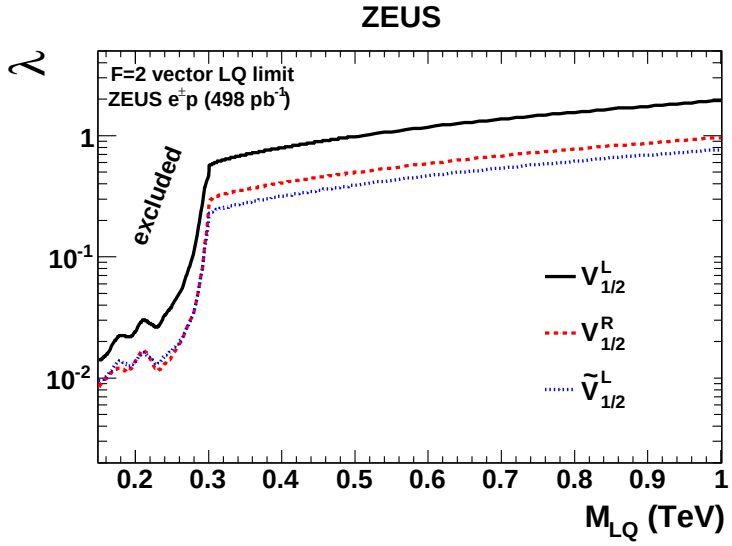

Figure 15: *Coupling limits, $\lambda_{\rm limit}$, as a function of LQ mass for vector F=2 BRW LQs. The areas above the curves are excluded according to Eq. (5).*

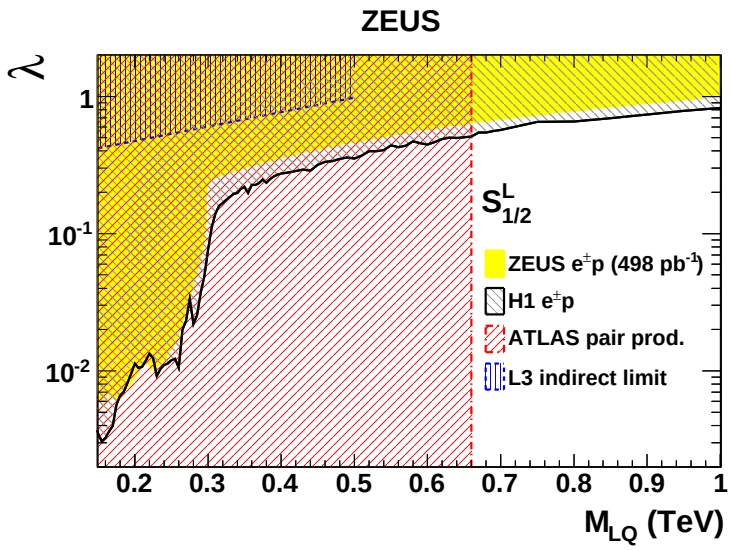

Figure 16: *Coupling limits as a function of LQ mass for the $S^L_{1/2}$ LQ from ATLAS, L3, H1 and ZEUS.*

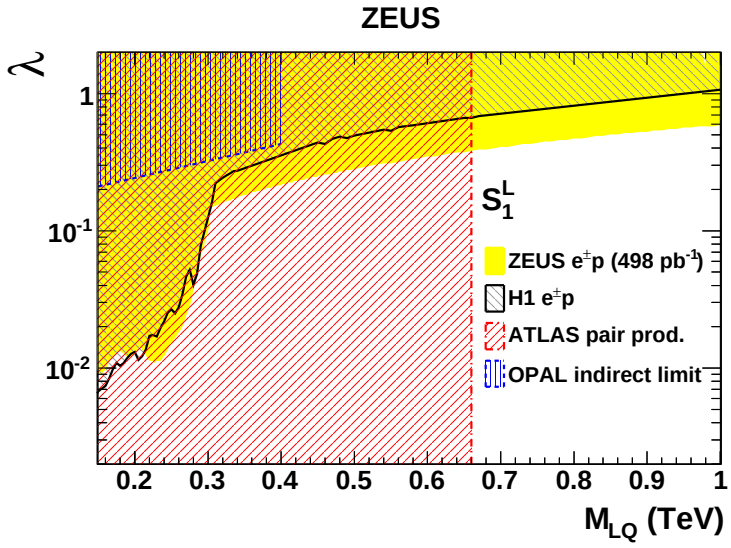

Figure 17: *Coupling limits as a function of LQ mass for the S^L_1 LQ from ATLAS, OPAL, H1 and ZEUS.*